ELSEVIER

International Journal of Mass Spectrometry 197 (2000) 243–252

International Journal of Mass Spectrometry

Direct ab initio dynamics study of the photoelectron detachment processes of the H_3O^- anion

Manabu Igarashi, Hiroto Tachikawa*

Division of Molecular Chemistry, Graduate School of Engineering, Hokkaido University, Sapporo 060-8628, Japan

Received 30 July 1998; accepted 19 November 1999

Abstract

Direct ab initio dynamics calculations on the photoelectron detachment processes of H_3O^- anion have been carried out by using HF/6-311G** full dimensional potential energy surface (PES). Total energy and the energy gradient of atoms were calculated in each time step. The excess energy was assumed to be zero at the starting point of the trajectory. The H_3O^- anion is composed of two isomers, $H^-(H_2O)$ and $OH^-(H_2)$ in which H^- and OH^- anions are solvated by H_2O and H_2 molecules, respectively. The present calculations indicated that the available energy, yielded by the electron detachment of $H^-(H_2O)$, is almost distributed into the relative translational energy between fragments. On the other hand, the available energy in an $OH^-(H_2)$ isomer is partitioned into both the relative translational mode and internal modes of the fragments, although the latter energy is minor. The excitation of internal modes of the products were observed for only the detachment process of the $OH^-(H_2)$ complex. These are due to the fact that the structure of solvent molecules (H_2O and H_2) in each complex is significantly close to that of free molecules whereas the PES of the neutral state is always repulsive. The mechanism of the electron detachment process of H_3O^- is discussed on the basis of theoretical results. (Int J Mass Spectrom 197 (2000) 243–252) © 2000 Elsevier Science B.V.

Keywords: Electron detachment; H_3O^-; Ab initio trajectory; Reaction dynamics

1. Introduction

The transition state (TS) is the most important region for determining in the product states in the reaction. Recently, several works for elucidating the electronic states and structures of the molecule around the TS have been made by means of a photoelectron detachment (PED) technique of molecular anions [1]. The PED technique is one of the best ways to elucidate the electronic states and structures in the vicinity of TS.

Recently, Neumark and co-workers have measured the PED spectra of H_3O^- anions [2]. The H_3O^- anion has two conformers corresponding to $H^-(H_2O)$ and $OH^-(H_2)$ [3]. The equilibrium points of H_3O^- are significantly close to TS of the hydrogen abstraction reaction from H_2 molecule by OH radical

$$OH + H_2 \rightarrow HO...H...H\ (TS) \rightarrow H_2O + H$$

if an electron is vertically removed from H_3O^- anion [4,5]. Hence, the measurement of the PED spectra of H_3O^- would provide direct information on the TS spectroscopy in the reaction of $OH + H_2$. They indicated that the PED spectra of H_3O^- originate from two reaction channels

* Corresponding author. E-mail: hiroto@eng.hokudai.ac.jp

PII S1387-3806(99)00261-4

$$H^-(H_2O) \xrightarrow[-e-]{hv} H + H_2O \quad (I)$$

$$OH^-(H_2) \xrightarrow[-e-]{hv} OH + H_2 \quad (II)$$

where $H^-(H_2O)$ is an anion in which H^- is solvated by a water, whereas OH^- is solvated by a H_2 molecule in $OH^-(H_2)$ anion. Their work indicated strongly that channel (I) is dominant at very low temperatures because the energy of the $H^-(H_2O)$ complex is slightly lower than that of $OH^-(H_2)$. On the other hand, at high temperatures (>200 K), the $OH^-(H_2)$ complex contributes to the PED spectra, although $H^-(H_2O)$ still contributes to the main peak. There is an activation barrier between the $H^-(H_2O)$ and $OH^-(H_2)$ complexes.

Theoretical treatment for the PED process of H_3O^- was carried out by Neumark and co-workers [2]. They calculated the wave packet on the potential energy surface obtained by ab initio molecular orbital calculations. The PED spectrum calculated by them is in reasonable agreement with the experiment, although the calculation was performed by using two-dimensional potential energy surface (PES).

In the present study, direct ab initio dynamics calculation is made for the PED process of H_3O^- in order to elucidate the product state distributions in channels I and II. The calculation was carried out on full-dimensional PES including all degrees of freedom, although the treatment is at the classical trajectory level. The main purpose of this study is to elucidate the available energy distribution in the PED products of H_3O^-.

2. Method of calculations

In general, the classical trajectory is performed on an analytically fitted potential energy surface as previously carried out [6]. However, it is not appropriate to predetermine the reaction surfaces of the present systems due to the large number of degrees of freedom ($3N - 6 = 12$, where N is number of atoms in the system). Therefore, in the present study, we applied the direct ab initio trajectory calculation with all degrees of freedom. Details of direct dynamics method is described elsewhere [7].

In the direct ab initio dynamics calculation, we used a 6-311G** basis set for the electron-detachment process of H_3O^- throughout. First, a trajectory calculation of the anion system H_3O^- was carried out in order to obtain the initial structures of the neutral H_3O radical. The HF/6-311G** optimized geometries of $H^-(H_2O)$ and $OH^-(H_2)$ were chosen as initial structures. At the start of the trajectory calculation, atomic velocities are adjusted to give two temperatures of 3 and 20 K. Temperature is defined by

$$T = \frac{1}{3N\,k}\left\langle \sum_{i=1}^{N} m_i v_i^2 \right\rangle$$

where N is number of atoms, v_i and m_i are velocity and mass of ith atom, and k is Boltzman constant. The equations of motion for n atoms in a molecule are given by

$$\frac{dQ_j}{dt} = \frac{\partial H}{\partial P_j}$$

$$\frac{\partial P_j}{\partial t} = -\frac{\partial H}{\partial Q_j} = -\frac{\partial U}{\partial Q_j}$$

where $j = 1$–$3N$, H is the classical Hamiltonian, Q_j is the Cartesian coordinate of jth mode, and P_j is the conjugated momentum. These equations were numerically solved by the Runge-Kutta method. No symmetry restriction was applied to the calculation of the gradients in the Runge-Kutta method. The time step size was chosen by 0.50 fs, and a total of 1000 steps was integrated for each dynamics calculation. The drift of the total energy is confirmed to be less than 0.1% throughout all steps in the trajectory.

In the direct ab initio dynamics calculations for the neutral H_3O radical, the optimized structures of $H^-(H_2O)$ and $OH^-(H_2)$ were first chosen as initial structures. Second, we chose 10 and 30 points at 20 and 3 K, respectively, from randomly selected points on the Franck-Condon (FC) region each of $H^-(H_2O)$ and $OH^-(H_2)$. A total of 40 trajectories for both the $H^-(H_2O)$ and the $OH^-(H_2)$ systems were run from the selected points on the FC region. The excess

Table 1
Ab initio geometries for stationary points of H_3O^- and H_3O (distances in angstroms and angles in degrees) calculated at the MP2/6-311++G**//MP2/6-311++G** level; MP2/aug-cc-pVDZ//MP2/aug-cc-pVDZ values are given in parentheses

Species	*r*(O–H1)	*r*(O–H3)	*r*(H1–H2)	∠H3–O–H1	∠O–H1–H2
$H^-(H_2O)$	1.023 (1.035)	0.961 (0.967)	1.442 (1.433)	98.8 (97.6)	170.3 (172.9)
$OH^-(H_2)$	1.943 (2.100)	0.965 (0.969)	0.768 (0.775)	135.3 (123.0)	173.6 (177.0)
H_3O^- (TS)	1.346 (1.281)	0.964 (0.971)	0.930 (1.001)	98.4 (99.2)	177.8 (178.7)
H_3O (TS)	1.332	0.969	0.813	97.3	162.3

energy of the system is assumed to be zero at the starting point of the trajectory calculation.

In order to obtain detailed structures and energetics of H_3O^- and H_3O systems, the ab initio MO calculations [8] were carried out at the Hartree-Fock (HF) and second order Møller-Plesset (MP2) levels of theory with 6-311G** and 6-311++G** basis sets.

3. Results

3.1. Ab initio MO calculations

3.1.1. Structures of the complexes

First, the geometries of H_3O^- composed of two isomers, $H^-(H_2O)$ and $OH^-(H_2)$, and of the neutral H_3O radical are optimized by means of the MP2/6-311++G** calculation. The optimized geometrical parameters are given in Table 1. The structure of H_3O^- is schematically illustrated in Fig. 1. The structures obtained in the present study are in good agreement with the results of MP4/6-311++G** calculations by Neumark and co-workers [2] and also of MP2/aug-cc-pVDZ calculations by Xanthes and Dunning [9]. Our calculation also results in a bent $OH^-(H_2)$ structure found by Ortiz [10].

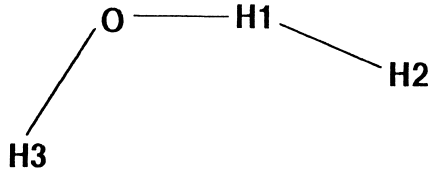

Fig. 1. Schematic structure and geometrical parameters of the H_3O^- complex.

3.1.2. Energetics

Total and relative energies for the stationary points and asymptotes of the H_3O^- anion and the neutral H_3O calculated at HF/6-311G** and MP2/6-311++G** are listed in Table 2. These results are in good agreement with those of the MP4/6-311++G** calculations by Neumark and co-workers [2].

For the anion system H_3O^-, the well of the $OH^-(H_2)$ complex is very shallow at both the HF/6-311G** and MP2/6-311++G** levels; the energy differences between the transition state and $OH^-(H_2)$ are 0.05 and 1.78 kcal/mol, respectively. The differ-

Table 2
Total energy (in atomic units) and relative energies (in electron volts) calculated for the H_3O^- and H_3O systems

	HF/6-311G**		MP2/6-311++G**	
Species	Total energy	Relative energy	Total energy	Relative energy
$H^- + H_2O$	−76.513 683 9	0.792	−76.780 531 9	0.837
$H^-(H_2O)$	−76.542 804 6	0.000	−76.811 296 9	0.000
H_3O^-TS	−76.515 449 9	0.744	−76.806 425 1	0.133
$OH^-(H_2)$	−76.515 523 5	0.742	−76.809 258 0	0.055
$OH^- + H_2$	−76.493 901 5	1.331	−76.800 510 4	0.294
$H + H_2O$	−76.546 821 8	0.000	−76.774 738 3	0.000
H_3O TS	−76.504 088 5	1.163	−76.725 371 3	1.343
$OH + H_2$	−76-543 226 4	0.978	−76.740 209 5	0.940

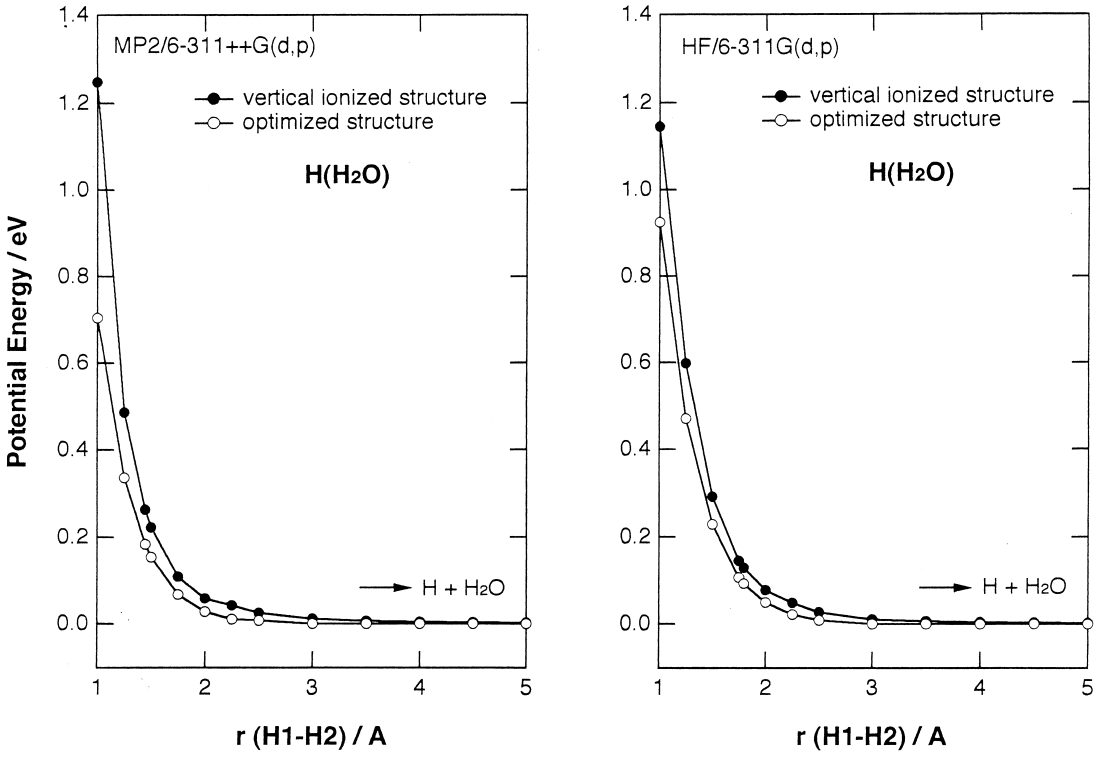

Fig. 2. Potential energy curves (PECs) for the lowest state of $H(H_2O)$ are calculated as a function of intermolecular distance r(H1–H2). The geometric parameters along r(H1–H2) are fully optimized (open circle) or fixed to that of anion $H^-(H_2O)$ (filled circle) on the calculation. Left and right panels are calculated at the MP2/6-311++G** and HF/6-311G** levels, respectively.

ence is changed to 0.30 kcal/mol if we consider zero point energies.

3.1.3. Potential energy curves

All PEC calculations were carried out at the HF/6-311G** and MP2/6-311++G** levels of theory. First, the PECs for the lowest state of $H(H_2O)$ were calculated as a function of intermolecular distance r(H1–H2). The geometric parameters except for r(H1–H2) are fully optimized or fixed to those of anion $H^-(H_2O)$ on the calculation. The PECs thus obtained are plotted in Fig. 2. The geometry optimization along r(H1–H2) shifts the PECs slightly for the low energy region, although energy lowering is quite small in the $H(H_2O)$ system. The PECs are strongly repulsive throughout. Similar calculations are also carried out at the HF/6-311G** level. The shape of the PECs calculated by HF/6-311G** is in good agreement with those obtained by MP2 calculations. These results strongly imply that the dynamics calculation at the HF/6-311G** level would provide qualitatively a reasonable result for the product state of fragments.

The PECs for the $OH(H_2)$ system are calculated in the same manner and plotted in Fig. 3. The shape of the PECs is repulsive, although a shallow minimum is found at 2.8 Å for the $OH(H_2)$ system. Similar minima are also seen in PECs calculated by the HF/6-311G** level. The shape of the PECs implies that, after vertical photoelectron detachment from two anion isomers to neutral H_3O surface, the complex would be dissociated directly to fragments. However, energy transfer and partitioning processes are still unknown. In Sec. 3.2, we study how the available energies distribute to the internal and intermolecular modes by means of ab initio direct dynamics method.

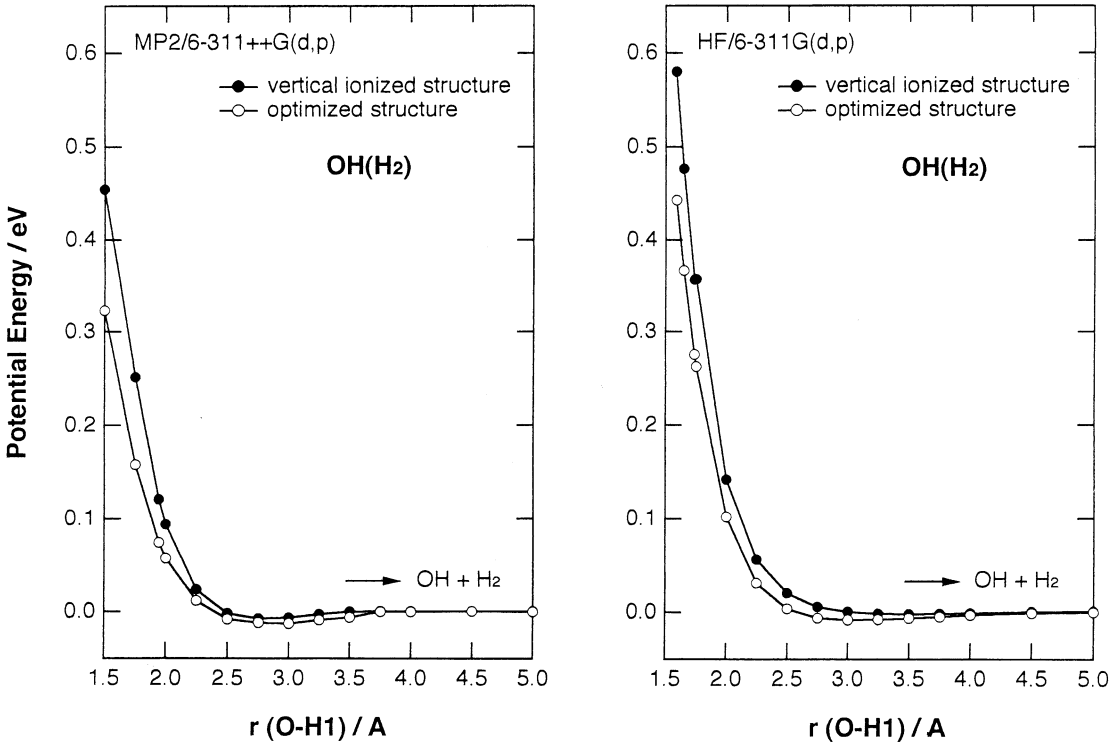

Fig. 3. PECs for the lowest state of $OH(H_2)$ are calculated as a function of intermolecular distance r(O–H1). The geometric parameters along r(O–H1) are fully optimized (open circle) or fixed to that of anion $OH^-(H_2)$ (filled circle) on the calculation. Left and right panels were calculated at the MP2/6-311++G** and HF/6-311G** levels, respectively.

3.2. Ab initio direct dynamics calculations

3.2.1. Structures of H_3O^- at finite temperatures

All trajectory calculations were carried out at the HF/6-311G** level of theory. First, the trajectory calculations for two isomers, $H^-(H_2O)$ and $OH^-(H_2)$, were made under constant temperature condition (3 K) in order to obtain the initial structures for both complexes. The results of the trajectory calculation are plotted in Fig. 4. Fig. 4(A) shows the intermolecular distances for both complexes calculated as a function of time. The distances for $H^-(H_2O)$ and $OH^-(H_2)$ complexes fluctuate at 1.77–1.82 Å for the H1–H2 distance and at 1.69–1.80 Å for the O–H1 distance, respectively. Similar calculations were performed at 20 K. As shown in Fig. 4(B), both distances, r(H1–H2) and r(O–H1), largely fluctuate at 20 K. In the $H^-(H_2O)$ complex, the distance of r(H1–H2) varies in the range of 1.69–1.92 Å.

The trajectory for $OH^-(H_2)$ at 20 K is much different than that at 3 K. In the case of this trajectory calculation, the simulation produced the $H^-(H_2O)$ complex as the final product. This is due to the fact that the energy barrier located in the middle of the $H^-(H_2O)$ and $OH^-(H_2)$ complexes is low enough to exceed the barrier height at 20 K. A total of 80 points on the H_3O^- PES are sampled for the initial geometries in the dynamics calculation of the H_3O system: 60 and 20 geometrical configurations are chosen from those obtained at 3 and 20 K, respectively.

3.2.2. Trajectories of the electron-detachment process in $H^-(H_2O)$

A sample trajectory for the electron-detachment process of $H^-(H_2O)$ at 3 K is given in Fig. 5. Potential energy (PE) plotted in Fig. 5(A) shows that the energy is suddenly low after 0.03 ps. After that, the PE

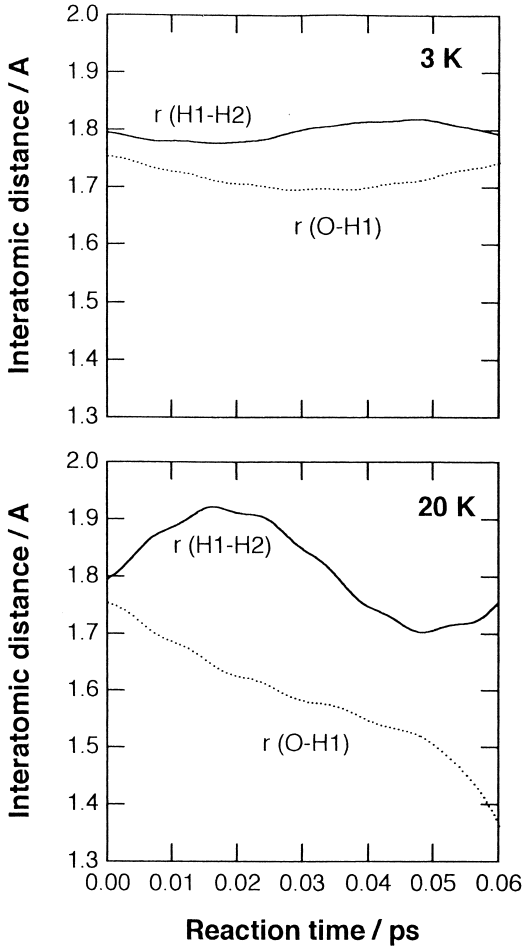

Fig. 4. Sample trajectories for two isomers, $H^-(H_2O)$ and $OH^-(H_2)$, calculated under the constant temperatures at (A) 3 and (B) 20 K. The intermolecular distances for $H^-(H_2O)$ and $OH^-(H_2)$ complexes are plotted by solid and broken lines, respectively.

periodically fluctuates and exhibits an average constant value at 0.05 ps. The interatomic distance of r(H1–H2) increases linearly with increasing reaction time, suggesting that H atom is rapidly escaping from H_2O after photodetachment. The relative translational energy estimated by Fig. 5(B) is 1.72 kcal mol^{-1}, which is 66% of the total available energy in the case of this sample trajectory. The internal bond distances of H_2O, r(O–H1) and r(O–H3), are hardly changed by photodetachment. The angle of H–O–H of H_2O [Fig. 5(C)] periodically vibrates with a normal amplitude. These results strongly indicate that the most of avail-

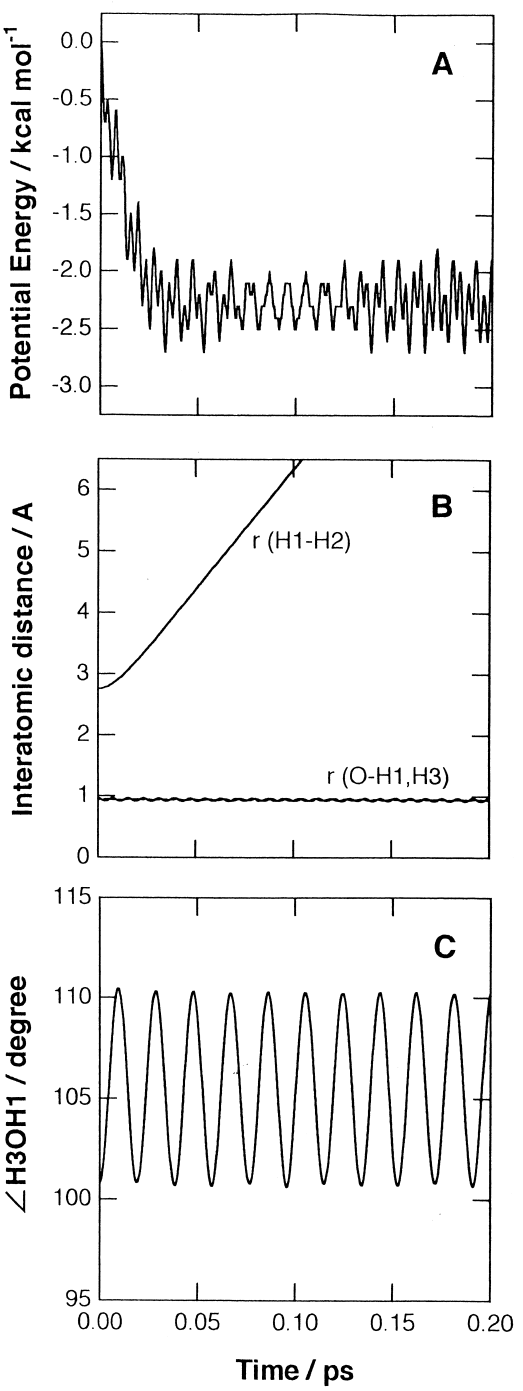

Fig. 5. A sample trajectory for photodetachment process of $H^-(H_2O)$ at 3 K plotted for (A) potential energy, (B) intermolecular distances, and (C) angle of H3–O–H1 of H_2O vs. time.

able energy efficiently converts to the relative translational energy between H and H_2O at 3 K.

3.2.3. Trajectories of the electron-detachment process in $OH^-(H_2)$

Fig. 6 shows the result of trajectory calculation for electron detachment of $OH^-(H_2)$. The potential (PE) of the system is suddenly down within a very short time region (<0.03 ps). After that, the PE largely fluctuates as shown in Fig. 6A. Time dependence of the interatomic distance for *r*(H1–H2) shows that the OH radical is rapidly separated from the H_2 molecule. The relative translational energy between the OH and H_2 fragments is estimated to be 4.57 kcal mol^{-1} in the case of this sample trajectory. This means that almost all available energy is partitioned into the relative translational energy. In fact, the internal modes, for example, *r*(O–H1), *r*(O–H3), and ∠H3–O–H1, are still in vibrational and rotational grand states in this sample trajectory, as clearly shown in Figs. 6(B) and 6(C).

3.2.4. Electron-detachment process at 20 K

The similar trajectory calculations at 20 K were made from the geometrical configurations of H_3O^- anions. The result for the $H^-(H_2O)$ complex at 20 K was very similar to that at 3 K: almost all available energy is partitioned into the relative translational energy. The internal modes were not enhanced by the electron-detachment process in $H^-(H_2O)$ at 20 K.

In the case of the $OH^-(H_2)$ complex, on the other hand, the result at 20 K is slightly different from the one at 3 K. Several trajectories, excited around the transition state for $OH^-(H_2)$ complexes, lead to the vibrational excited products. In such cases, the available energy is partitioned into the vibrational mode of H_2 and the relative available energy between the H_2 and OH fragments. The vibrational mode for H_2 was excited up to $v = 1$, although the population of H_2 ($v = 1$) was less than 10% in the present calculations.

3.2.5. Populations of the relative translational energies

In previous sections, we showed the sample trajectory for each complex $H^-(H_2O)$ or $OH^-(H_2)$. The

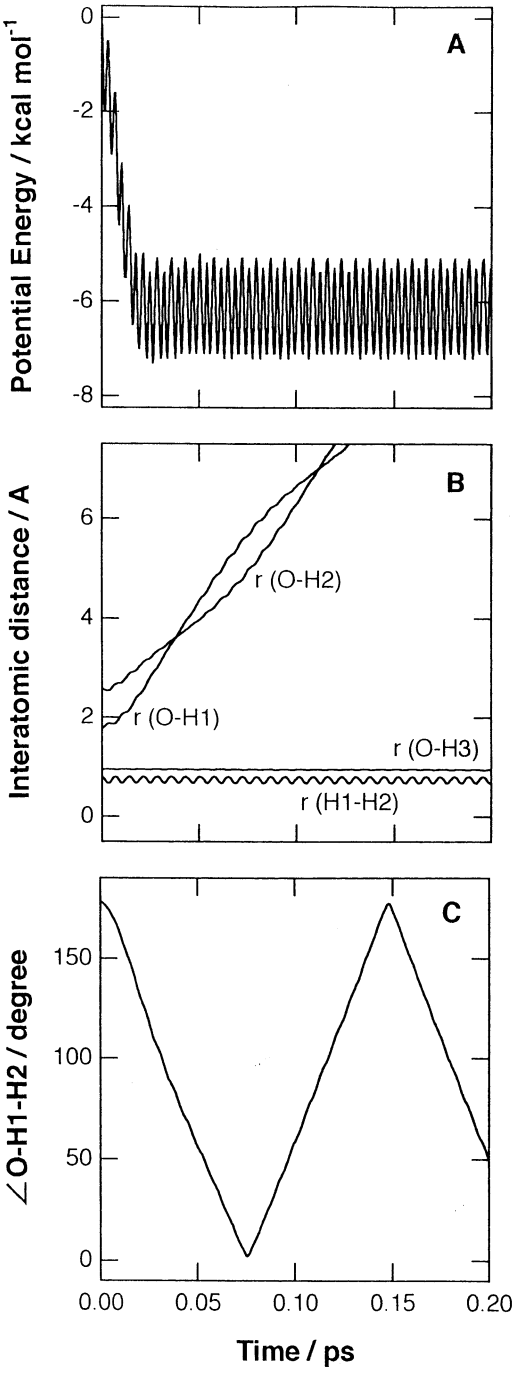

Fig. 6. A sample trajectory for the photodetachment process of $OH^-(H_2)$ at 3 K plotted for (A) potential energy, (B) intermolecular distances, and (C) angle of O–H1–H2 vs. time.

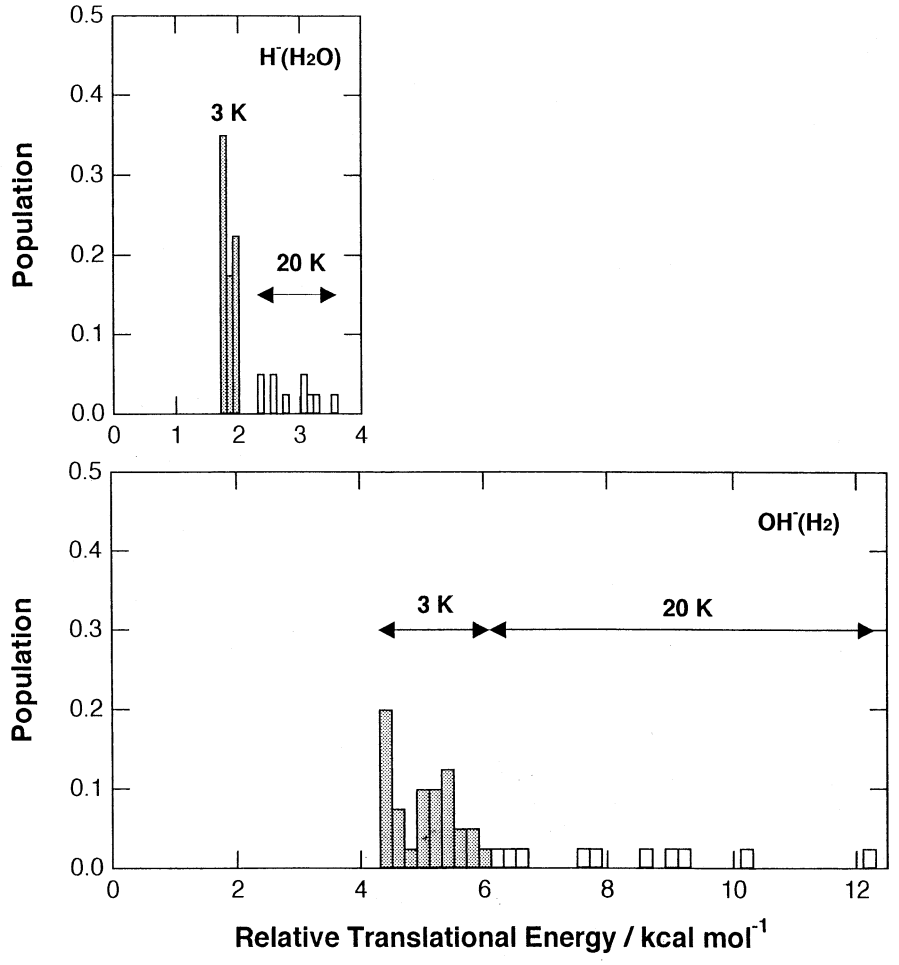

Fig. 7. Populations of relative translational energy between fragments formed by the photodetachment processes, $H^-(H_2O) \rightarrow H + H_2O$ (upper) and $OH^-(H_2) \rightarrow OH + H_2$ (lower).

available energy after electron detachment was mainly partitioned into the relative translational energy between the fragments in both complexes. In this section, the distributions of the translational energy are presented as a summary of the trajectory calculations.

The above mentioned direct ab initio dynamics calculations were performed up to the number of trajectory of 40 for each complex. For each complex, 30 and 10 trajectories were run at 3 and 20 K, respectively. A total of 80 trajectories were run. The results of the translational energy distribution are given in Fig. 7 as a population diagram. The upper and lower panels express the populations for $H^-(H_2O)$ and $OH^-(H_2)$ complexes, respectively. In both complexes, the populations at 3 K are almost concentrated in shallow energy ranges: 1.8–2.0 kcal mol^{-1} for $H^-(H_2O)$ and 4.2–6.0 kcal mol^{-1} for $OH^-(H_2)$ complexes. For the $H^-(H_2O)$ complex at 20 K, the population of relative translational energy is slightly shifted to a high energy region, whereas the distribution is slightly spread. On the other hand, the populations calculated for the $OH^-(H_2)$ complex at 20 K are widely distributed from 6.0 to 12.4 kcal mol^{-1}.

4. Concluding remarks

In the present study, the available energy distributions of the products formed by the photodetachment of the H_3O^- anion have been investigated by means of the direct ab initio dynamics method with the full-dimensional PES, including all degrees of freedom. All atoms are treated as classical particles moving on full-dimensional PES. The calculation showed that almost available energy is partitioned into the relative translational energy between fragments. This is due to the fact that structures of H_2O in the $H^-(H_2O)$ complex and H_2 in the $OH^-(H_2)$ complex are significantly close to those of free molecules. The structures of solvent molecules (H_2O and H_2) are hardly affected by the solvation of the anion in the complexes. We also showed that the product state distribution is largely affected by temperature. This is due to the fact that the ratio of $H^-(H_2O)$ and $OH^-(H_2)$ complexes is gradually varied as a function of temperature.

Neumark and co-workers carried out wave packet dynamics on the photodetachment process of H_3O^- [2]. They treated two-dimensional (2D) dynamics in the calculation. The present classical trajectory calculation on the full-dimensional PES shows that the 2D wave-packet treatment is adequate to describe qualitatively the dynamics of H_3O^-. Very recently, Clary et al. calculated the photodetachment spectrum of H_3O^- by a quantum scattering method with the rotating bond approximation [11]. Three active degrees of freedom (two stretching vibrations and one bending mode) are considered in the calculation. They suggested that photodetachments of $H^-(H_2O)$ and $OH^-(H_2)$ lead to $H + H_2O$ and $OH + H_2$ products, respectively. In the latter case, a progression of a band associated with different OH internal states in the $OH + H_2$ product channel was identified. These results are in reasonable agreement with the present results obtained by classical treatment. However, wave function for vibrational excited states needs as an initial wave packet to obtain a more detailed feature [12].

We have introduced several approximations to treat the reaction dynamics and to calculate the potential energy surface. First, we assumed that the neutral complex has no excess energy at the initial step of the trajectory calculation (time = 0.0 ps). This may cause a slight change of reaction time and energy distribution in the fragments. In the case of higher excess energy, the internal modes of the fragments may be more enhanced. This effect was not considered in the present calculations. It should be noted therefore that the present model is limited in case of no excess energy. Second, we used the HF/6-311G** multidimensional potential energy surface in the trajectory calculations throughout. A more accurate wave function may provide deeper insight in the dynamics. Despite several assumptions introduced here, the results enable us to obtain valuable information on the mechanism of photoelectron detachment processes in H_3O^-.

Acknowledgements

The authors are indebted to the Computer Center at the Institute for Molecular Science (IMS) for the use of the computing facilities. The authors also acknowledge partial support from a Grant-in-Aid from the Ministry of Education, Science, Sports and Culture of Japan.

References

[1] (a) R.B. Metz, A. Weaver, S.E. Bradforth, T.N. Kitsopoulos, D.M. Neumark, J. Phys. Chem. 94 (1990) 1377; (b) S.E. Bradforth, D.W. Arnold, D.M. Neumark, J. Chem. Phys. 99 (1993) 6345.

[2] E. deBeer, E.H. Kim, D.M. Neumark, R.F. Gunion, W.C. Lineberger, J. Phys. Chem. 99 (1995) 13627.

[3] (a) D. Cremer, E. Krafa, J. Phys. Chem. 90 (1986) 33; (b) G. Chalasinski, R.A. Kendall, J. Simons, J. Chem. Phys. 87 (1987) 2965; (c) S.S. Xantheas, T.H. Dunning Jr., J. Phys. Chem. 96 (1992) 7505; (d) T.M. Miller, A.A. Viggiano, A.E.S. Miller, R.A. Morris, M. Henchman, J.F. Paulson, J.M.V. Doren, J. Chem. Phys. 100 (1994) 5706.

[4] (a) S.P. Walch, T.H. Dunning Jr., J. Chem. Phys. 72 (1980) 1303; (b) G.C. Schatz, H. Elgersma, Chem. Phys. Lett. 73 (1980) 21; (c) D.C. Clary, J. Chem. Phys. 96 (1992) 3656; (d) D. Wang, J.M. Bowman, J. Chem. Phys. 96 (1992) 8906; (e) H. Szichman, I. Last, A. Baram, M. Baer, J. Chem. Phys. 97 (1993) 6436; (f) D. Neuhauser, J. Chem. Phys. 100 (1994) 9272; (g) D.H. Zhang, Z.H. Zhang, J. Chem. Phys. 101 (1994)

1146; (h) U. Manthe, T. Seideman, W.H. Miller, J. Chem. Phys. 101 (1994) 4759; (i) N. Balakrishnan, G.D. Billing, Chem. Phys. Lett. 233 (1995) 145; (j) D.H. Zhang, J.C. Light, J. Chem. Phys. 104 (1996) 4544.

[5] (a) G.C. Light, J.H. Matsumoto, Chem. Phys. Lett. 58 (1978) 578; (b) F.P. Tully, A.R. Ravishankara, J. Phys. Chem. 84 (1980) 3126; (c) R. Zellner, W. Steinert, Chem. Phys. Lett. 81 (1981) 568; (d) G.P. Glass, B.K. Chaturvedi, J. Chem. Phys. 75 (1981) 2749; (e) J.R. Fisher, J.V. Michael, J. Phys. Chem. 94 (1990) 2465; (f) A. Sinha, M.C. Hsiao, F.F. Crim, J. Chem. Phys. 94 (1991) 4928; (g) K. Kessler, K. Kleinermanns, Chem. Phys. Lett. 190 (1992) 145; (h) R.C. Oldenborg, G.W. Loge, D.M. Harradine, K.R. Winn, J. Phys. Chem. 96 (1992) 8426; (i) M. Alagia, N. Balucani, P. Casavecchia, D. Stranges, G.G. Volpi, J. Chem. Phys. 98 (1993) 2459; (j) R.A. Loomis, R.L. Schwartz, M.I. Lester, J. Chem. Phys. 104 (1996) 6984.

[6] (a) H. Tachikawa, J. Chem. Phys. 108 (1998) 3966; (b) H. Tachikawa, K. Ohnishi, T. Hamabayashi, H. Yoshida, J. Phys. Chem. A 101 (1997) 2229; (c) H. Tachikawa, J. Phys. Chem. 99 (1995) 225; (d) M. Abe, Y. Inagaki, L.L. Springsteen, Y. Matsumi, M. Kawasaki, H. Tachikawa, J. Phys. Chem. 98 (1994) 12641; (e) H. Tachikawa, T. Hamabayashi, H. Yoshida, J. Phys. Chem. 99 (1995) 16630; (f) H. Tachikawa, H. Takamura, H. Yoshida, J. Phys. Chem. 98 (1994) 5298; (g) H. Tachikawa, A. Ohtake, H. Yoshida, J. Phys. Chem. 97 (1993) 11944.

[7] (a) H. Tachikawa, J. Phys. Chem. A 101 (1997) 7475; (b) H. Tachikawa, J. Phys. Chem. 100 (1996) 17090; (c) H. Tachikawa, K. Komaguchi, Int. J. Mass Spectrom. Ion Processes 164 (1997) 39; (d) Program code of the direct ab initio dynamics calculation was made by our group.

[8] Ab initio MO calculation program: GAUSSIAN 94, M.J. Frisch, G.W. Trucks, H.B. Schlegel, P.M.W. Gill, B.G. Johnson, M.A. Robb, J.R. Cheeseman, T. Keith, G.A. Petersson, J.A. Montgomery, K. Raghavachari, M.A. Al-Laham, V.G. Zakrzewski, J.V. Ortiz, J.B. Foresman, J. Cioslowski, B.B. Stefanov, A. Nanayakkara, M. Challacombe, C.Y. Peng, P.Y. Ayala, W. Chen, M.W. Wong, J.L. Andres, E.S. Replogle, R. Gomperts, R.L. Martin, D.J. Fox, J.S. Binkley, D.J. Defrees, J. Baker, J.P. Stewart, M. Head-Gordon, C. Gonzalez, J.A. Pople, GAUSSIAN 94, revision D.3, Gaussian, Inc., Pittsburgh, PA, 1995.

[9] S.S. Xantheas, T.H. Dunning Jr., J. Chin. Chem. Soc. 42 (1995) 241.

[10] J.V. Oritz, J. Chem. Phys. 91 (1989) 7024.

[11] D.C. Clary, J.K. Gregory, M.J.T. Jordan, E. Kauppi, J. Chem. Soc., Faraday Trans. 93 (1997) 747.

[12] R.N. Dixon, H. Tachikawa, Mol. Phys. 97 (1999) 195.